J Mater Sci (2008) 43:1270–1277
DOI 10.1007/s10853-007-2252-z

Surface grain boundary engineering of shot-peened type 304 stainless steel

Osama M. Alyousif · Dirk L. Engelberg · Thomas J. Marrow

Received: 6 September 2007 / Accepted: 23 October 2007 / Published online: 4 December 2007

Abstract The effect of thermal annealing on shot-peened Type 304 stainless steel has been examined using electron backscatter diffraction (EBSD) and X-ray diffraction (XRD). The objective was to evaluate the potential for surface property control by grain boundary engineering. The near surface microstructure of shot-peened material showed a gradual change of the grain boundary character distribution with depth. Twin (Σ3) and higher order twin grain boundaries (Σ9, Σ27) identified closer to the shot-peened surface had significant deviations from their optimum misorientation. The subsequent application of annealing treatments caused depth-dependent changes of the near surface microstructure, with variations in grain size, low Σ CSL grain boundary populations and their deviation from optimum misorientation. Microstructure developments were dependent on the applied heat treatment, with the near surface microstructures showing similarities to microstructures obtained through bulk thermo-mechanical processing. Shot peening, followed by annealing, may therefore be used to control the near surface microstructure of components.

Introduction

Grain boundaries with a high density of coinciding lattice atom sites, characterized as low Σ grain boundaries in the coincidence site lattice model (CSL) [1], can be resistant to intergranular corrosion and stress corrosion cracking [2–4]. Although the CSL description is an incomplete description of grain boundaries, which are best described using five-parameters for the relative crystal orientations and the grain boundary plane [5, 6], it is widely used for convenience.

The concept of increased microstructure resistance by grain boundary design and control, which involves the development of microstructures with increased fractions of "special" low Σ CSL boundaries (i.e. Σ1–Σ29), was introduced by Watanabe [7]. Palumbo and coworkers developed this idea into a robust process, known as grain boundary engineering (GBE) [8, 9].

GBE has been implemented mainly by thermo-mechanical processing of bulk materials, using either strain recrystallization or strain annealing processes [10]. The choice of temperature and treatment sequence is generally dependent on intrinsic material characteristics and can be tailored for individual purposes. For example, by controlling thermo-mechanical process parameters such as the amount of introduced strain and recrystallization temperature, Lin et al. [11] and Lehockey et al. [12] have improved the intergranular corrosion resistance in nickel-based alloy 600 and alloy 625 by a multi-step (iterative) strain recrystallization process. Kumar et al. [13] and Schuh et al. [14] showed the influence of similar multi-step treatments on the evolution and connectivity of potentially resistant grain boundary networks in alloy 600. Thaveeprungsriporn et al. [15] and King et al. [16] have reported the evolution of twin variant grain boundaries ($\Sigma 3^n$, $0 < n \leq 3$) in Type 304 stainless steel and copper using iterative and single-step strain annealing processes, respectively. Low-strain (i.e., less than 10%) thermo-mechanical processing with annealing treatments in the lower homogeneous temperature regime has also shown the

O. M. Alyousif (✉)
Department of Mechanical Engineering, College of Engineering & Petroleum, Kuwait University, P.O. Box 5969, Safat 13060, Kuwait
e-mail: alyousif@kuc01.kuniv.edu.kw

D. L. Engelberg · T. J. Marrow
Materials Performance Centre, School of Materials, The University of Manchester, Manchester M1 7HS, UK

potential to significantly increase the fraction of low Σ CSL boundaries in austenitic stainless steel [17, 18] and nickel-base alloy 800 [19]. Engelberg et al. observed three consecutive stages in the microstructure development with progressive annealing periods after low-strain processing [18]. GBE of Type 304 austenitic stainless steel has been shown to improve the resistance to intergranular stress corrosion crack nucleation, through the development of crack bridging [20–23]. Crack bridging was caused by non-sensitized grain boundary segments, which tended to be produced by the growth of annealing twins. Increasing the fraction of twins increased the frequency of such bridges. Modelling of this mechanism of stress corrosion cracking shows that grain refinement and an increase in the fraction of resistant boundaries, gave an increase in SCC resistance, particularly for short cracks [20–23].

Thermo-mechanical processing, either by cold rolling reduction or tensile straining followed by annealing treatments, is commonly used for grain boundary engineering. However, there is a range of new processes under investigation. These include, for instance, the application of external shear stresses [24] and the superposition of magnetic fields during annealing [25, 26], or the application of new process routes, such as equal-channel angular pressing [27]. An alternative process route for GBE comprises the introduction of relatively shallow surface strains, followed by thermal treatments, since it is also desirable to grain boundary engineer the surface of complex shaped components. For instance, Wang et al. have improved the mechanical properties and corrosion resistance of Type 304 by sand-blasting and annealing [28]. The application of shot peening without subsequent annealing has also been reported to improve the corrosion resistance through the formation of a nanocrystallized layer on the surface of Type 316L and 1Cr18Ni9Ti stainless steels [29, 30]. The depth of the modified microstructure was of the order of 30 μm. Limoges et al. [31] showed that the corrosion resistance of alloy 625 can be significantly increased through the application of high-intensity shot peening cycles, each followed by short recrystallization heat treatments. It is believed that the later iterative "beating and heating" process produces populations of up to 60–70% "special" grain boundaries in the near surface region [32].

The introduction of gradual surface plastic strains with increasing depth, and the influence of subsequent annealing treatments on the nearsurface microstructure development are, however, not fully understood. The aim of this study was to investigate the effect of shot peening and the influence of subsequent annealing on the development of grain boundary engineered nearsurface microstructures in Type 304 austenitic stainless steel. Comparisons with bulk thermo-mechanically processed microstructures of the same material are also introduced.

Experimental

The material used in this study was a mill annealed Type 304 austenitic stainless steel. The chemical composition (wt.%) is given in Table 1. A rectangular specimen, measuring approximately 100 mm × 100 mm × 12.5 mm was treated by conventional shot-peening. Samples were removed for analysis in the as shot-peened condition and after subsequent annealing treatments at either 900 °C for 30 min or 1,050 °C for 10 min. After annealing, all specimens were cooled in air to room temperature. Bulk processed specimens of the same Type 304 material were uni-directionally cold rolled with a reduction of 15%, followed by the same annealing treatments as the shot-peened samples. Table 2 gives an overview of samples investigated.

Residual stress measurements of the shot-peened material were carried out with a Bruker X-ray diffractometer, using Cr–Kα radiation at 30 keV. This analysis is based on the $\sin^2\psi$ method for which the residual stress was calculated by using five ψ-angles from 0 to 40°. A Young's modulus E = 210 GPa and a Poisson's ratio of 0.3 was used for the conversion of the measured strains into elastic stress. Residual stress depth profiling was achieved by successively electropolishing an area of 1 cm^2 in 92% (vol.) acetic acid and 8% (vol.) perchloric acid. Measurements were carried out to a depth of 320 μm, with intervals of 20–30 μm. The residual stress data obtained as a function of depth were not corrected for stress relaxation which occurred as a result of material removal.

A Philips X-Pert X-ray diffractometer with Cu-Kα radiation at 50 keV was used to investigate the presence of martensite in the near surface region on the perpendicular section of the heat-treated and as-received shot-peened samples.

Table 1 Chemical composition (wt.%) of the Type 304 stainless steel plate

Cr	Ni	Si	Mn	C	S	N	Fe
18.15	8.60	0.45	1.38	0.055	0.005	0.038	Bal.

Table 2 Process route of investigated samples

Sample	Process route	Heat treatment
0	As-received	–
1	Shot Peened	–
2a	Shot Peened	900 °C/30 min
2b	Shot Peened	1,050 °C/10 min
3a	15% Cold Rolled	900 °C/30 min
3b	15% Cold Rolled	1,050 °C/10 min

An HKL-EBSD system, interfaced to a Philips XL-30 FEG-SEM, was used for EBSD analysis, by using a step size of 2 μm, with typical exposure times of 50–70 ms. The shot-peened and annealed, and shot-peened samples were assessed in sections perpendicular and parallel to the treated surface. Perpendicular assessments were carried out in three adjacent areas measuring 100 μm × 400 μm, located directly below the shot-peened surface, in order to determine the microstructure development with depth. Parallel assessments were carried out at depths of 30 ± 10 μm and 90 ± 10 μm, with respect to the original shot-peened surface. All bulk-processed specimens were assessed along the middle fibre in sections perpendicular to the rolling direction, with an area of at least 500 μm × 500 μm.

Analysis of the EBSD data was carried out with an in-house developed software (Vmap [33]). Grain size measurements considered all high-angle (>15°) grain boundaries, including twin grain boundaries (Σ3). Uncertainties of grain size measurements include one standard deviation, typically from at least 30 linear intercept measurements. The Brandon deviation criterion ($\theta = \alpha\,\theta_o\,\Sigma^{-1/2}$, $\alpha = 1$) was used to define the maximum allowed deviation from exact CSL misorientation [34]. Grain boundaries up to Σ29 were regarded as low-Σ CSL boundaries, and are given as number fractions. The grain boundaries were divided into different groups, comprising Low Angle Grain Boundaries (LAGB–Σ1), twin (Σ3) and higher order twin grain boundaries (Σ9 and Σ27). All LAGBs were characterized between 2° and 15°. All data sets were also assessed with a tighter deviation in the Brandon criterion ($\alpha = 0.5$), to determine the proximity of the twin (Σ3) and higher order twin population (Σ9, Σ27) to their optimum misorientation. This assessment thus excludes a fraction of the grain boundaries that are geometrically further away from their optimum misorientation.

Results and discussion

As-received parent material

The as-received material (Sample 0) had a grain size of 15.8 ± 2.5 μm. The GBCD and proximity data of the twin variant grain boundaries are given in Table 3. Moderate fractions of low-Σ CSL grain boundaries (Σ1–Σ29) were present in the parent material before shot peening, with mostly Σ3 twin grain boundaries, and only a low proportion of higher order twins (Σ9, Σ27) and LAGBs (Σ1). The low population of LAGBs reflects the mill annealed, recrystallized material condition. Low fractions of higher order twin grain boundaries imply that the microstructure had not been modified by multiple twinning, since high populations of Σ9 and Σ27 grain boundaries are generally indicative of grain boundary engineered microstructures [10]. Most twin (>90%) and higher order twin grain boundaries (≈80%) had deviations close to their optimum misorientation.

Table 3 Gain boundary character distribution and proximity of the as-received parent material

Σ1–Σ29	Σ3	Σ9, Σ27	LAGB (Σ1)
37.4 ± 1.6 %	23.0 ± 1.2 % (9.3 %)	4.7 ± 0.3 % (21.6 %)	4.0 ± 0.5 %

The values in brackets show the relative fraction of grain boundaries outside the tighter deviation criterion ($\alpha = 0.5$), and gives information about the deviation of grain boundaries. Uncertainties reported include the minimum and maximum of two assessed regions

Effect of shot peening

Residual stress depth profiles of the shot-peened sample (Sample 1) in the longitudinal and transverse directions are shown in Fig. 1. The residual stresses are compressive up to a depth in excess of 300 μm, with the highest stress close to the shot-peened surface (region a). No transition to tensile stresses was observed in the regions close to the surface, and the data analysis was terminated due to inconsistency in signal intensity at a depth of 320 μm. The peak widths at half maximum (FWHM) for the five ψ-angles are shown in Fig. 2. The peak width is highest at the surface and decreases with increasing depth. This indicates that the maximum plastic deformation is located at the surface of the material. Variations of the peak width for the five ψ-angles can be attributed to inhomogeneous surface strain distributions.

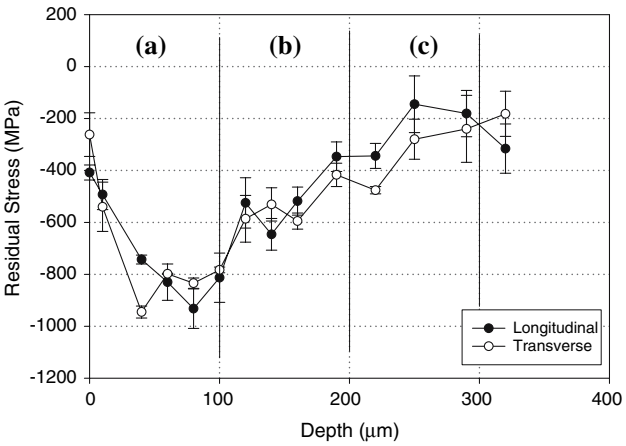

Fig. 1 Residual stress depth profiles on the shot peened sample (sample 1) in the longitudinal and transverse directions. The depth profile is divided into 3 regions (a,b,c) of 100 μm depth each

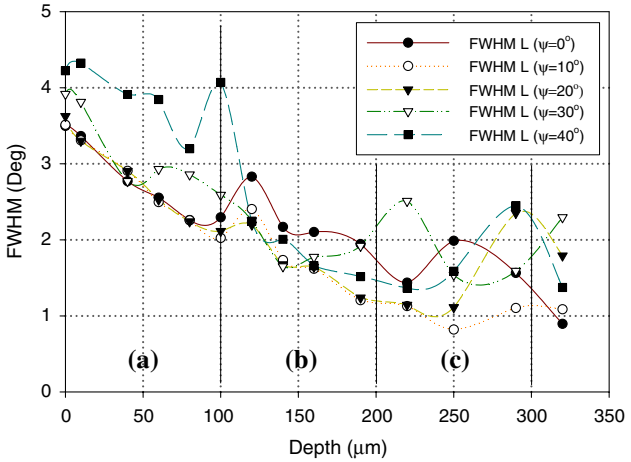

Fig. 2 Peak widths at half maximum (FWHM) for the five- ψ angles with respect to the shot-peened surface. The three regions of Fig. 1 (a,b,c) are superimposed

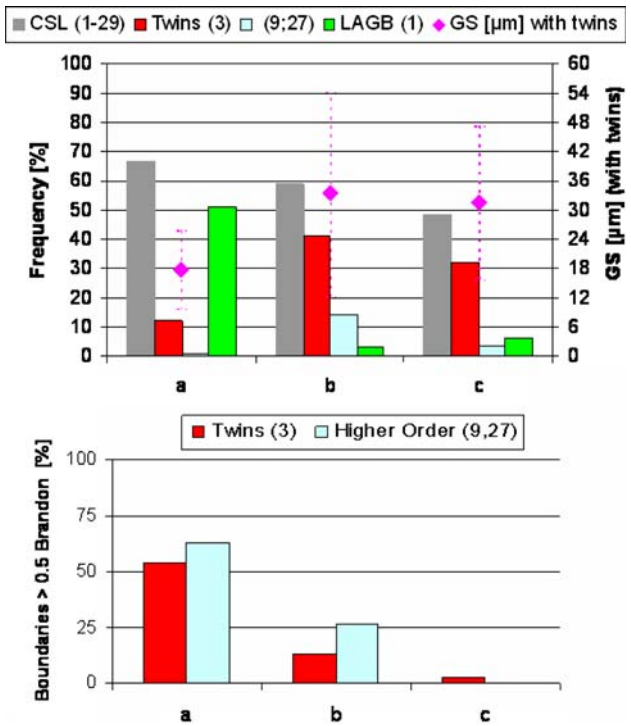

Fig. 3 (a) GBCD of the three horizontal regions (a,b,c) of sample 1. Each region has a height of 100 μm, with region (a) closest to the shot-peened surface. (b) Relative proximity of the twin and higher order twin fractions, showing the population of boundaries further away from their optimum misorientation

The magnitude and location of the observed residual stress and FWHM profiles highlight the gradual change of introduced strains and plastic deformation with depth. Significant strain is only observed within 200 μm of the surface. The potential for strain-driven microstructural changes is therefore the highest in a region close to the shot-peened surface. The obtained data are in reasonable agreement with literature data of other shot-peened Type 304 materials [35, 36]. XRD measurements at the surface of the samples for phase identification revealed no martensite in the microstructure of the material, with detected peaks corresponding to the austenite phase only.

An EBSD map of the grain boundary network of peened sample (Sample 1) was taken perpendicular to the top edge of the shot-peened surface. The map is divided into three horizontal regions with 100 μm height (a, b, c) and the GBCD data with average corresponding grain size and proximity data for each of the regions are summarized in Fig. 3. Adjacent to the surface, the grain size was approximately 18 ± 8 μm, increasing to approximately 30 ± 20 μm in the bulk microstructure. Clusters of small grains, located directly beneath the shot-peened surface and the relatively small assessment area, are probably the reasons for the large variations in grain size observed. Increased fractions of LAGBs are also apparent in the region close to the shot-peened surface. The GBCD shows that the total fraction of low-Σ CSL grain boundaries is the highest near the surface (68%). This is due to the high fraction of LAGBs introduced through the shot peening, which dominate the other boundary distributions. Region b and c have significantly reduced fractions of LAGBs, with twin fractions of approximately 40 and 30%, respectively. An increased population of higher-order twin grain boundaries (Σ9, Σ27) is apparent in region b. This may either be related to a transition of the highly strained surface layer to the base material, or more likely microstructural heterogeneities of the small assessment area. Close to the shot-peened surface, most twin (Σ3) and higher order twin (Σ9, Σ27) grain boundaries have deviations far off their optimum misorientation. This is likely to be related to an accumulation of dislocations at grain boundaries, producing local lattice rotations [37, 38].

An EBSD grain boundary map of a section parallel to the shot-peened surface at a depth of 90 ± 10 μm is shown in Fig. 4. The microstructure had a low CSL (Σ1–29) grain boundary fraction of 74.6%, with 63.3% LAGBs (Σ1) and only 9.4% (Σ3) twins, with a grain size of 24 μm. The population of LAGBs clearly dominated the microstructure at this depth. Reassessment of the data, by excluding the LAGB population, gave a twin (Σ3) frequency of ≈19%, from which a total of 72% had deviations far away from their exact misorientation (larger than 0.5 Brandon). Figure 4 also highlights some inhomogeneously distributed regions with high densities of LAGBs, and accumulation of LAGBs at some high-angle grain boundaries. The assessed section at a depth of 90 ± 10 μm yielded reasonable results (>80% indexing) with an exposure time at each analysis point of 300 ms, followed by frame averaging. A similar approach was applied to the parallel section at a

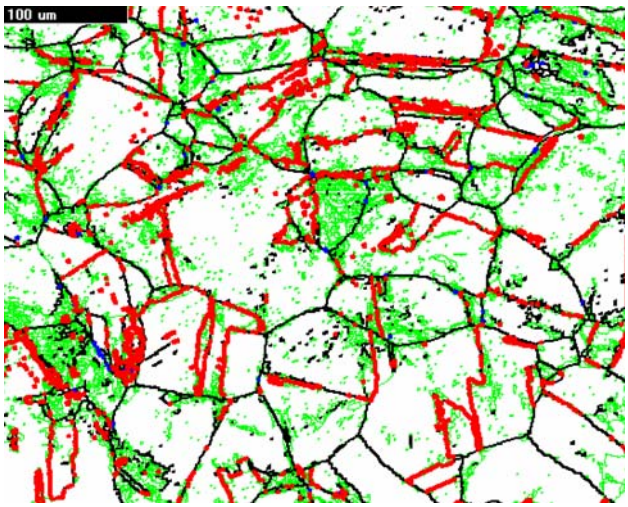

Fig. 4 EBSD grain boundary map parallel to the shot-peened surface of sample 1 at a depth of 90 ± 10 μm. LAGBs are shown with thin green lines, twins and higher order twins with thick red and blue lines, respectively, and all remaining grain boundaries with black lines

depth of 30 ± 10 μm, but yielded indexing rates below 30%. This was attributed to the presence of significantly increased plastic strains closer to the shot-peened surface.

The gradual change of the residual stress and FWHM profiles with depth is therefore reflected in the effect of LAGBs on the different grain boundary populations of the three assessed regions, and the decrease in measured deviations of the twin and higher order twin grain boundaries.

Effect of annealing after shot peening

Shot-peened samples were annealed at 900 °C for 30 min (Sample 2a,) and 1,050 °C for 10 min (Sample 2b). XRD analysis did not detect any martensite in these microstructures after annealing. EBSD grain boundary maps of both samples were taken perpendicular to the shot-peened surface. The grain size, GBCD and deviation data of the perpendicular regions are summarized in Figs. 5 and 6, respectively.

The total fractions of low Σ CSL boundaries in the three perpendicular sections after annealing at 900 °C are similar with, however, a higher fraction of LAGBs closer to the shot-peened surface (Fig. 5, region a). This indicates that the annealing treatment at 900 °C was not able to completely recover the introduced plastic strain. A comparison between region b and c of the shot-peened sample (Fig. 3) with the comparable regions after annealing at 900 °C (Fig. 5) shows that no significant grain growth has occurred. The average grain size near the surface of sample 2a remains slightly smaller than in the bulk, with clusters of smaller grains surrounded by larger grains. The grain size

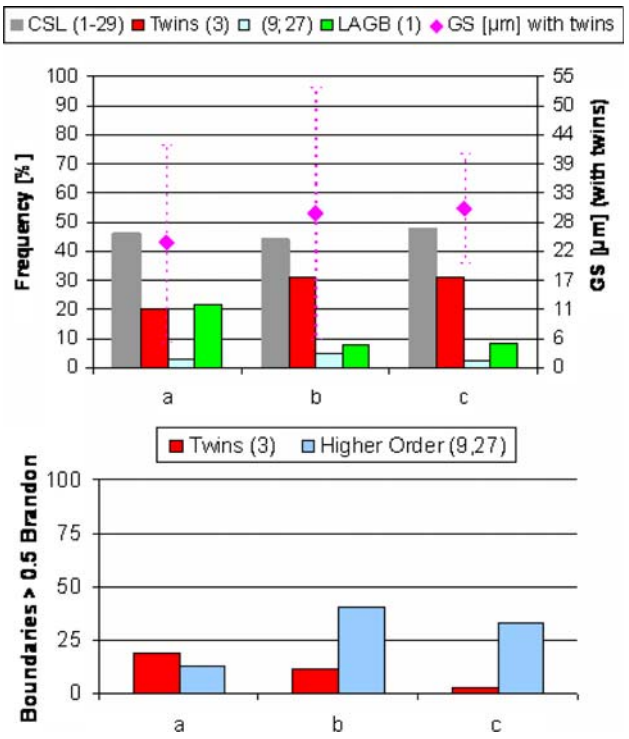

Fig. 5 (a) GBCD of the three horizontal regions (a,b,c) of sample 2a. Each region has a height of 100 μm, with region (a) closest to the shot-peened surface. (b) Relative proximity of the twin and higher order twin fractions, showing the population of boundaries further away from their optimum misorientation

differences may have been caused by in-homogeneously distributed strain, which can result in local recrystallization [39, 40]. This is consistent with the presence of increased populations of LAGBs in some grains, whereas other grains appear free of LAGBs.

All three perpendicular regions of sample annealed at 1,050 °C indicate similar microstructures. This is also apparent in the GBCD in Fig. 6. The strains introduced through shot peening have been relieved by annealing, which is also reflected in significantly decreased LAGB populations. The measured grain size was around 30 μm in all assessed regions, with, however, significant deviations.

The annealing treatment had also affected the proximity data for the twin variant population. There is a slight trend of decreasing deviation with depth for the twin boundary population after annealing at 900 °C (Fig. 5), whereas almost all twins are close to their optimum misorientation after annealing at 1,050 °C (Fig. 6). The higher order twin fraction show more exact deviations closer to the shot-peened surface. However, there is small number of higher order twin grain boundaries in these samples, and these data are judged not to be significant. The small population of higher order twin boundaries in Figs. 5 and 6 indicate that both annealed microstructures did not undergo multiple twinning.

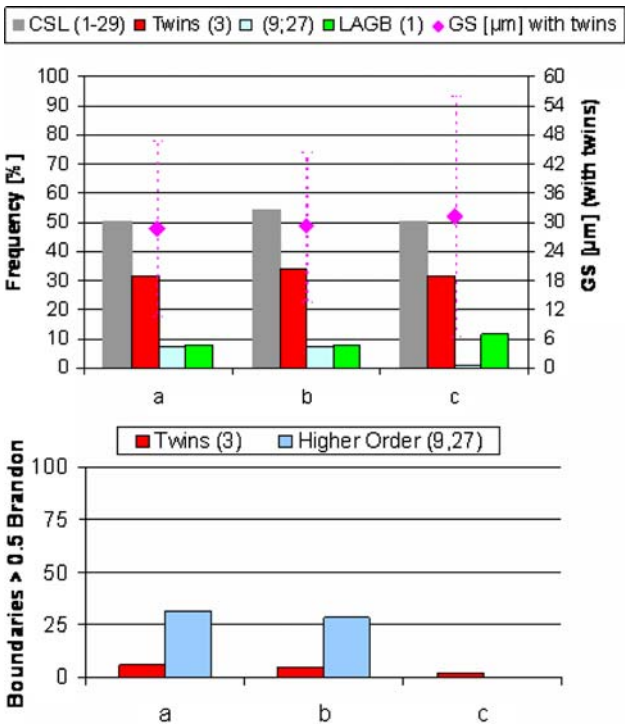

Fig. 6 (a) GBCD of the three horizontal regions (a,b,c) of sample 2b. Each region has a height of 100 µm, with region (a) closest to the shot-peened surface. (b) Relative proximity of the twin and higher order twin fractions, showing the population of boundaries further away from their optimum misorientation

Figures 7 and 8 show parallel sections of both annealed samples at a depth of 30 µm and 90 µm, respectively. Figure 9 gives the corresponding grain sizes and GBCDs. A comparison between both microstructures shows significant differences. The lower annealing temperature (Sample 2a) yields smaller grain sizes, with even a significant decrease at a depth of 90 µm. This effect of depth may be related to slower recrystallization kinetics with decreasing plastic deformation (Fig. 2), in particular with heat treatments in the lower recrystallization temperature regime [39, 40]. In contrast, annealing at 1,050 °C gave similar grain sizes and GBCDs at both assessed depths. These observations confirm the results of the perpendicular assessment (Figs. 5 and 6), which indicated large variations in the three assessed regions of sample 2a, but not in sample 2b. The minor differences in grain size and measured GBCDs between the perpendicular and parallel assessments are attributed to the gradual change of microstructure with depth, and the smaller assessment areas in the perpendicular sections.

Figure 9 shows a direct comparison of the microstructure characteristics after bulk thermo-mechanical processing and shot peening with annealing. A reduction of 15%, followed by an annealing treatment at 1,050 °C for 10 min gave similar microstructure characteristics as the same heat treatment after shot peening at a depth of 30 µm and 90 µm (Sample 2b).

The observed variations of the microstructures show the possibility to develop a range of surface modified microstructures through the introduction of nearsurface strains by peening with subsequent annealing treatments. The resultant microstructure in the vicinity of the surface after annealing at 1,050 °C, for example, is relatively insensitive to the level of plastic strain. In this work, the applied heat treatments were not tailored to induce multiple twinning. These can be achieved using small strains and similar annealing temperatures in bulk samples, although there is an effect of strain path on the required time for the onset of multiple twinning [41]. Further study is therefore required to identify the necessary conditions for multiple twinning in peened samples. The work presented here has demonstrated, however, that a combination of controlled introduction of surface strains with annealing has the

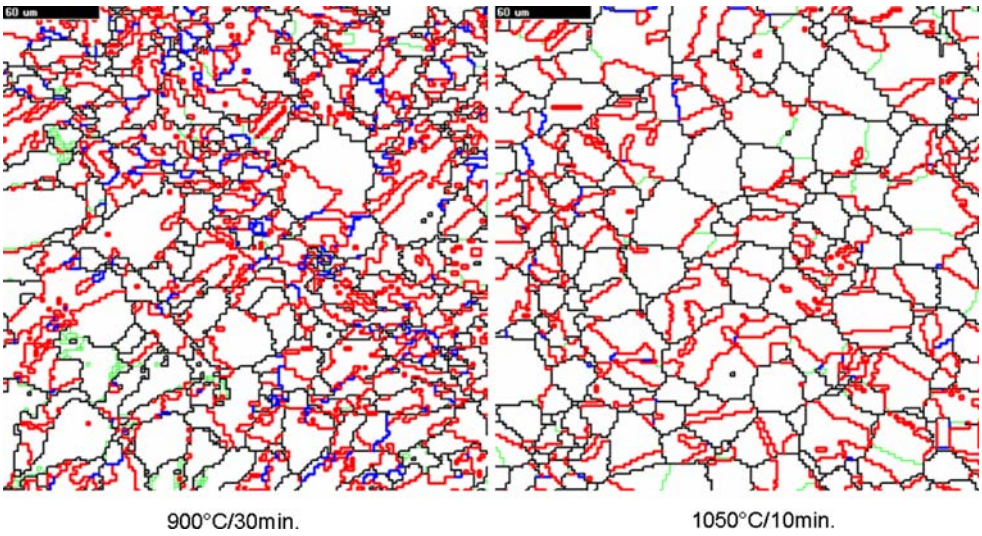

Fig. 7 EBSD grain boundary map parallel to the shot-peened surface of sample 2a and sample 2b at a depth of 30 ± 10 µm. LAGBs are shown with thin green lines, twins and higher order twins with thick red and blue lines, respectively, and all remaining grain boundaries with black lines

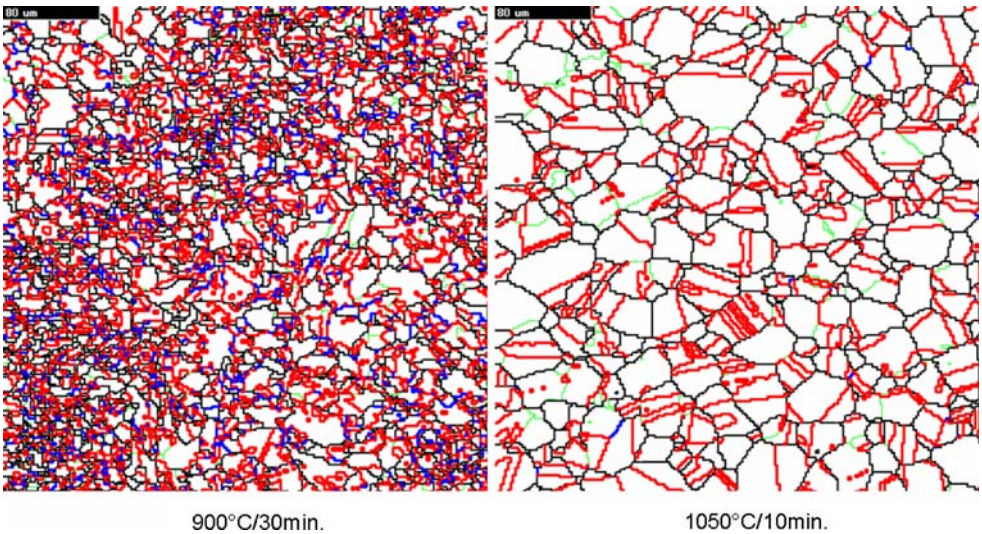

Fig. 8 EBSD grain boundary map parallel to the shot-peened surface of sample 2a and sample 2b at a depth of 90 ± 10 μm. LAGBs are shown with thin green lines, twins and higher order twins with thick red and blue lines, respectively, and all remaining grain boundaries with black lines

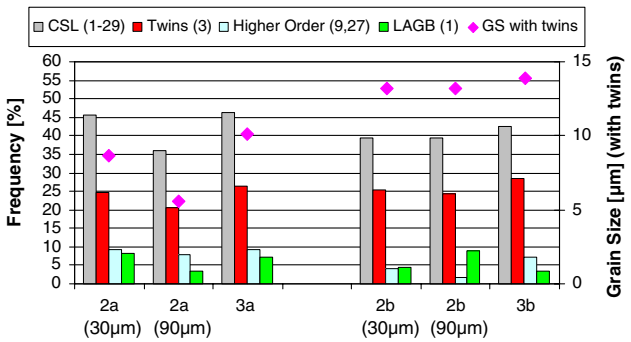

Fig. 9 GBCD of parallel regions of sample 2a and 2b at a depth of 30 ± 10 μm and 90 ± 10 μm. The GBCD of the bulk thermo-mechanical processed samples (Sample 3a, 3b) are shown for comparison

potential for surface grain boundary control in stainless steels. In the current work, a depth of around 100 μm was modified. It is likely that deeper strain profiles, for instance through the application of deep rolling [35], may be utilized to twin modify surface layers to a greater depth.

Conclusions

- Shot peening of Type 304 austenitic stainless steel induced a gradual change of grain size and grain boundary character distribution with depth.
- Twin (Σ3) and higher order twin (Σ9, Σ27) grain boundaries showed larger deviations from their optimum misorientation closer to the shot-peened surface. High fractions of low angle grain boundaries are also measured, due to the introduction of plastic strain.
- Subsequent annealing at 900 °C produced strong microstructure variations with depth, whereas annealing at 1,050 °C gave relatively uniform microstructure characteristics, comparable to those achieved by cold rolling and annealing of bulk samples.
- Combined shot peening and annealing may be used to surface modify the microstructure of Type 304 austenitic stainless steel.

Acknowledgements The authors are grateful for the support of Rolls-Royce (Marine) Ltd. The authors are grateful to Metal Improvement Company for conducting the peening of the 304 stainless steel. The authors are also grateful for the technical assistance from Judith Shackleton with the X-ray diffraction measurements and Lai Mei Li with the plastic strain measurements.

References

1. Grimmer H, Bollmann W, Warrington DH (1974) Acta Crystallogr A30:197
2. Gertsman VY, Bruemmer SM (2001) Acta Mater 49:1589
3. Bi HY, Kokawa H, Jie Wang Z, Shimada M, Sato YS (2003) Scripta Mater 49(3):219
4. Palumbo G, Aust KT (1990) Acta Metall Mater 38(11):23343
5. Randle V (2006) Scripta Mater 54:1011
6. Rohrer GS, Randle V, Kim C-S, Hu Y (2006) Acta Mater 54:4480
7. Watanabe T (1984) Res Mech 11:47
8. Palumbo G (1997) Patent 5,702,543—Thermomechanical Processing of Metallic Materials. United States
9. Palumbo G (1998) Patent 5,817,193—Metals Having Improved Resistance to Intergranular Stress Corrosion Cracking. United States
10. Randle V (1999) Acta Mater 47(15–16):4187
11. Lin P, Palumbo G, Erb U, Aust KT (1995) Scripta Metall Mater 33(9):1387
12. Lehockey EM, Palumbo G, Lin P (1998) Metall Mater Trans 29A:3069
13. Kumar M, King WE, Schwartz AJ (2000) Acta Mater 48:2081
14. Schuh CA, Kumar M, King WE (2003) Acta Mater 51:687
15. Thaveeprungsriporn V, Sinsrok P, Thong-Aram D (2001) Scripta Mater 44:67

16. King WE, Schwartz AJ (1998) Scripta Mater 38(3):449
17. Shimada M, Kokawa H, Wang ZJ, Sato YS, Karibe I (2002) Acta Mater 50(9):2331
18. Engelberg DL, Humphreys FJ, Marrow TJ (2007) J Microsc In Press
19. Tan L, Allen TR (2005) Metall Mater Trans 36A(7):1921
20. Jivkov AP, Stevens NPC, Marrow TJ (2006) Acta Mater 54:3493
21. Jivkov AP, Marrow TJ (2007) Theor Appl Fract Mech 48(3):187
22. Jivkov AP, Stevens NPC, Marrow TJ (2007) J Pressure Vessel Technol T ASME In Press
23. Jivkov AP, Stevens NPC, Marrow TJ (2006) Comp Mater Sci 38:442
24. Winning M (2006) Scripta Mater 54:987
25. Molodov DA, Konijnenberg PJ (2006) Scripta Mater 54:977
26. Watanabe T, Tsurekawa S, Zhao X, Zuo L (2006) Scripta Mater 54:969
27. Furukawa M, Horita Z, Langdon TG (2005) J Mater Sci 40:909
28. Wang XY, Li DY (2002) Electrochim Acta 47:3939
29. Liu G, Lu J, Lu K (2000) Mater Sci Eng A286:91
30. Wang T, Yu j, Dong B (2006) Surf Coat Technol 200:4777
31. Limoges DL, Palumbo G, Lin PK (2002) Patent 6,344,097 B1—Surface Treatment of Austenitic Ni-Fe-Cr-Based Alloys for Improved Resistance to Intergranular Corrosion and Cracking. United States
32. Lindsay JH (2004) Plat Surf Finish 91(7):1
33. Humphreys FJ (2001) Vmap—orientation mapping and quantitative metallography by EBSD. Manchester Materials Science Centre, The University of Manchester, Manchester
34. Brandon DG (1966) Acta Metall 14:1479
35. Altenberger I, Scholtes B, Martin U, Oettel H (1999) Mater Sci Eng A264:1
36. Renzhi W, Xaingbin L, Yuanfa Y (1985) In: Niku-Lari A (ed) Advances in surface treatments: technology, applications, effects, vol 2. Pergamon Press, pp 161–170 (ISBN 0080325351)
37. Kumar M, Schwartz AJ, King WE (2001) Mater Sci Eng A309–310:78
38. Thomson CB, Randle V (1997) Acta Mater 45(12):4909
39. Iino Y (1992) J Mater Sci Lett 11:1253
40. Iino Y, Kim TY, Mun SD (1996) Wear 199:211
41. Randle V, Jones R, Marrow J, Engelberg D (2008) Effect of Strain Path and Annealing on Development of Resistance to Intergranular Degradation in Austenitic Stainless Steel. ICOTOM 15. Pittsburgh: TMS